Electronic Supplementary Material (ESI) for ChemComm.

Supporting Information

Boosting efficient ambient nitrogen oxidation by a well-dispersed Pd on MXene electrocatalyst

Wei Fang, Chengfeng Du, Min Kuang, Mengxin Chen, Wenjing Huang, Hao Ren, Jianwei Xu,* Armin Feldhoff,* and Qingyu Yan*

S1. Experimental details

S1.1 Electrocatalysts synthesis

$Ti_3C_2T_x$ MXene nanosheets were synthesized according to the literature.[S1] Briefly, LiF was added to a 6 M HCl aqueous solution. Subsequently, Ti_3AlC_2 powders prepared by solid state reaction were slowly added into the above solution. The reacted mixture was then held at 40 ^oC for 45 h and afterwards washed with ultra pure water, followed by centrifugation, and decanting, until the supernatant reached a pH value of ~6. The obtained precipitates were ultra-sonicated in an ice-bath for 8 h. Finally, the supernatant was collected by centrifugation and freeze dried. Pd-MXene (Pd-MX) hybrid was prepared by the adsorption-annealing strategy.[S2] $Pd(OAc)_2$ was first dissolved in acetone, and then MXene sheets were dispersed into the above solution. The mixture was dried at 60 ^oC under vacuum and finally heat treated in 5% H_2-Ar at 800 ^oC for 2 h. The Pd loading mass was ~2 wt.% of the product.

S1.2 Materials characterization

The phase structures of the materials were determined by X-ray diffraction (XRD, D8 Advance, Bruker-AXS, with Cu Ka radiation) in the 2θ range 5-80^o with a step width of 0.02^o. The morphologies of electrocatalysts were observed by a field-emission scanning electron microscopy (FESEM, JEOL JSM-7600F) operated at 5 kV and an atomic force microscopy (AFM, Bruker D8 SPM). The Pd-MX electrocatalyst was also investigated at incident electron energy of 200 kV in a field-emission transmission electron microscopy (FETEM, JEOL JEM-2100F). The microscope was operated as scanning TEM (STEM) and high-resolution TEM (HRTEM). The elemental information of samples were analyzed by X-ray photoelectron spectroscopy (XPS, Kratos Axis SUPPA), energy dispersive X-ray spectroscopy (EDXS) and electron energy loss spectroscopy (EELS). Inductively coupled plasma (ICP) data was collected on an Optima

7300 DV instrument.

S1.3 Electrode preparation

Typically, 5 mg of electrocatalysts and 50 μL of 5 wt.% Nafion solution were dispersed in 450 μL of ethanol by sonicating for 1 h to form a homogenous ink. Then the as-prepared ink was loaded onto a carbon paper with an area of 1×1 cm^2 and dried under vacuum condition overnight. The obtained mass loading was 0.25 mg cm^{-2} (for NOR test using $^{14}N_2$).

S1.4 Electrochemical NOR measurements

All electrochemical nitrogen oxidation reaction (NOR) tests were carried out at room temperature in a two-compartment H-type cell, which was separated by a Nafion 117 membrane (DuPont). Before the tests, the Nafion membrane was pre-treated in 3% H_2O_2 solution and 5% H_2SO_4 solution as well as ultra-pure (UP) water in sequence. Between each tests, the Nafion membrane was also boiled in UP water to remove the possible trapped contamination, and the electrolyte on both sides of the soaked Nafion membrane was monitored by ion chromatograph before NOR tests as well. The high-purity N_2 (99.9995%), Ar (99.9995%) and $^{15}N_2$ isotope (98 atom % ^{15}N) gas were prepurified by passage through a 5% H_2SO_4 solution and a silica gel sorbent tube to remove any possible sources of N contamination, and subsequently bubbled through the electrolyte for at least half hour before NOR tests. The gas flow rate of N_2 and Ar was fixed at 30 mL min^{-1}. The flow rate of $^{15}N_2$ was 5 mL min^{-1} due to the limited supply. Electrochemical NOR measurements were conducted with a Solartron electrochemical station and employed by the three-electrode system including the electrocatalysts on carbon paper as the working electrode, carbon rod as the counter electrode and Ag/AgCl (in 3 M KCl solution) electrode as the reference electrode. The volume of electrolyte was 30 mL on both sides of Nafion membrane respectively. Cyclic voltammetry (CV) was performed with N_2 feeding in a 0.01 M Na_2SO_4 solution at a scan rate of 5 mV s^{-1}. For NOR experiments, galvanostatic tests were performed in the N_2-saturated 0.01 M Na_2SO_4 electrolyte with continuous N_2 feeding in a range of current density from 0.1 mA cm^{-2} to 0.5 mA cm^{-2}. For the electrochemical impedance (EIS) measurements, the frequency was swept in a range of 10^6-0.01 Hz with a perturbation alternating current amplitude of 10 mV at open circuit condition. Additionally, the concentration of produced nitrate was systematically detected and quantified by ion chromatography (930 compact IC Flex, Metrohm). Furthermore, for $^{15}N_2$ isotope labelling experiment, after 10 h of $^{15}N_2$ electro-oxidation (loading mass = 1 mg for electrode), the obtained $^{15}NO_3^-$ solution was subjected to concentration treatment, then determined by ^{15}N nuclear magnetic resonance (NMR, JEOL ECA400). D_2O was used as the solvent, and the reaction time of NMR tests for all samples was 11 hours with 11000 scans.

The yield rate of nitrate production was calculated by the following equation:

$$r_{NO_3^-} = (c \times V)/(t \times m)$$ Equation 1

where c is the measured nitrate mass concentration, V is the volume of the electrolyte, t is the electrochemical oxidation reaction time, and m is the loading mass of the electrocatalysts.

The Faradaic efficiency of nitrate yield can be calculated as follow:

$$FE_{NO_3^-} = (5F \times c \times V)/(M \times Q)$$ Equation 2

where F is the Faraday constant, c is the measured nitrate mass concentration, V is the volume of the electrolyte, M is relative molecular mass of nitrate, and Q is the total charge passed through the electrode during electrolysis.

S2. Supporting figures and table

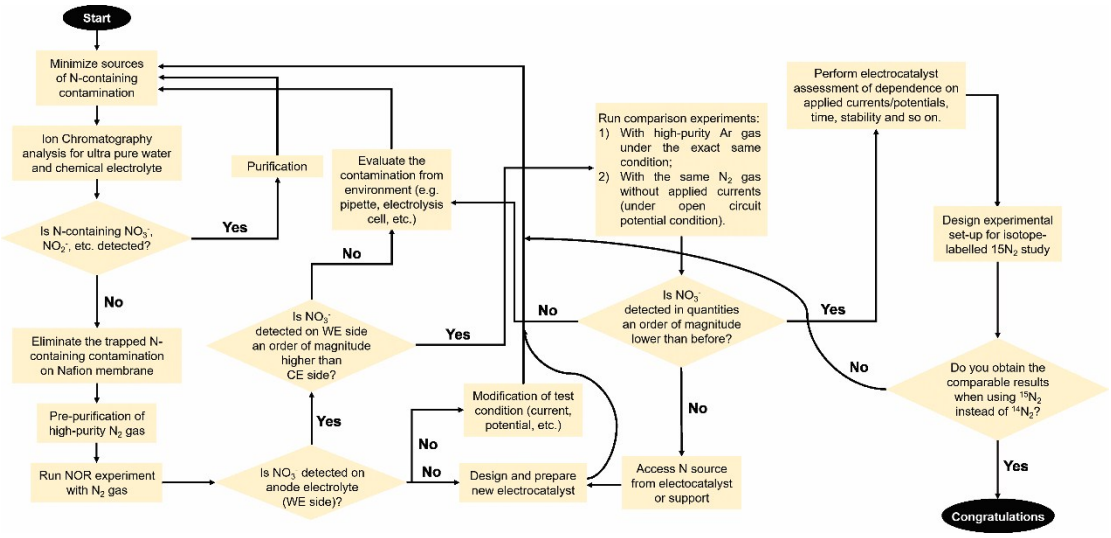

Fig. S1 Our protocol for the measurement of electrochemical nitrogen oxidation.

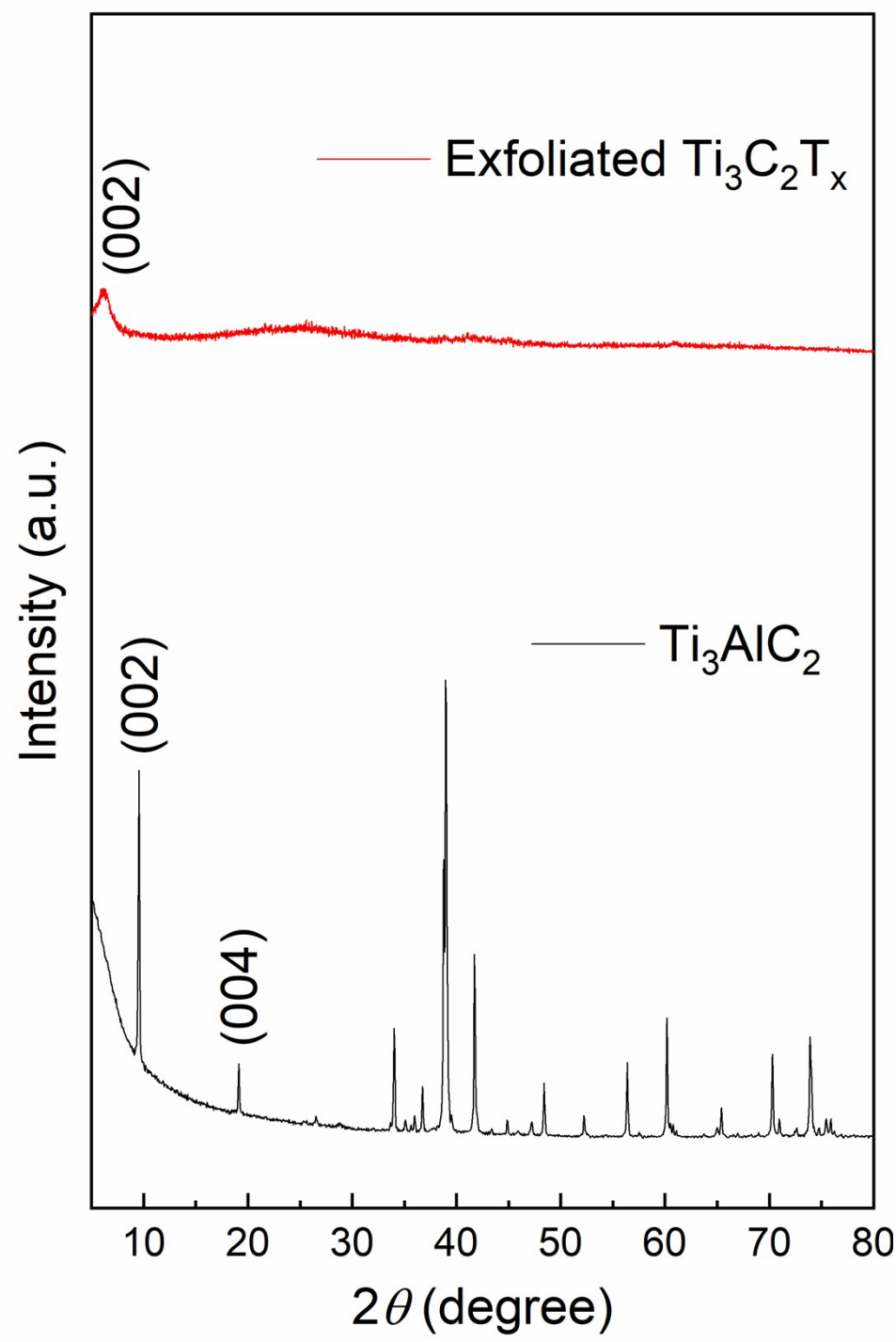

Fig. S2 XRD patterns of as-synthesized Ti_3AlC_2 and exfoliated $Ti_3C_2T_x$.

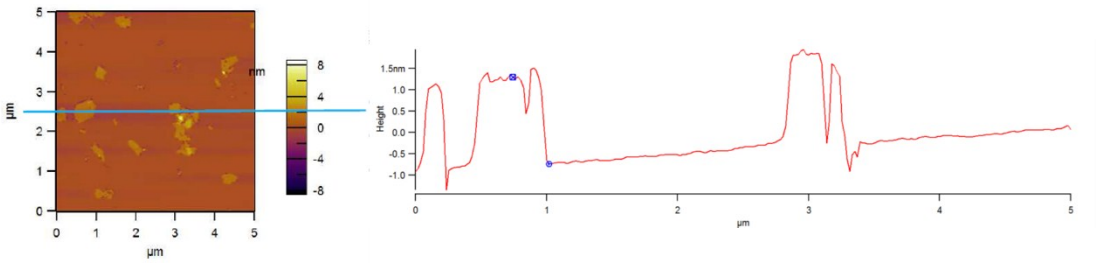

Fig. S3 AFM image of MXene nanosheet.

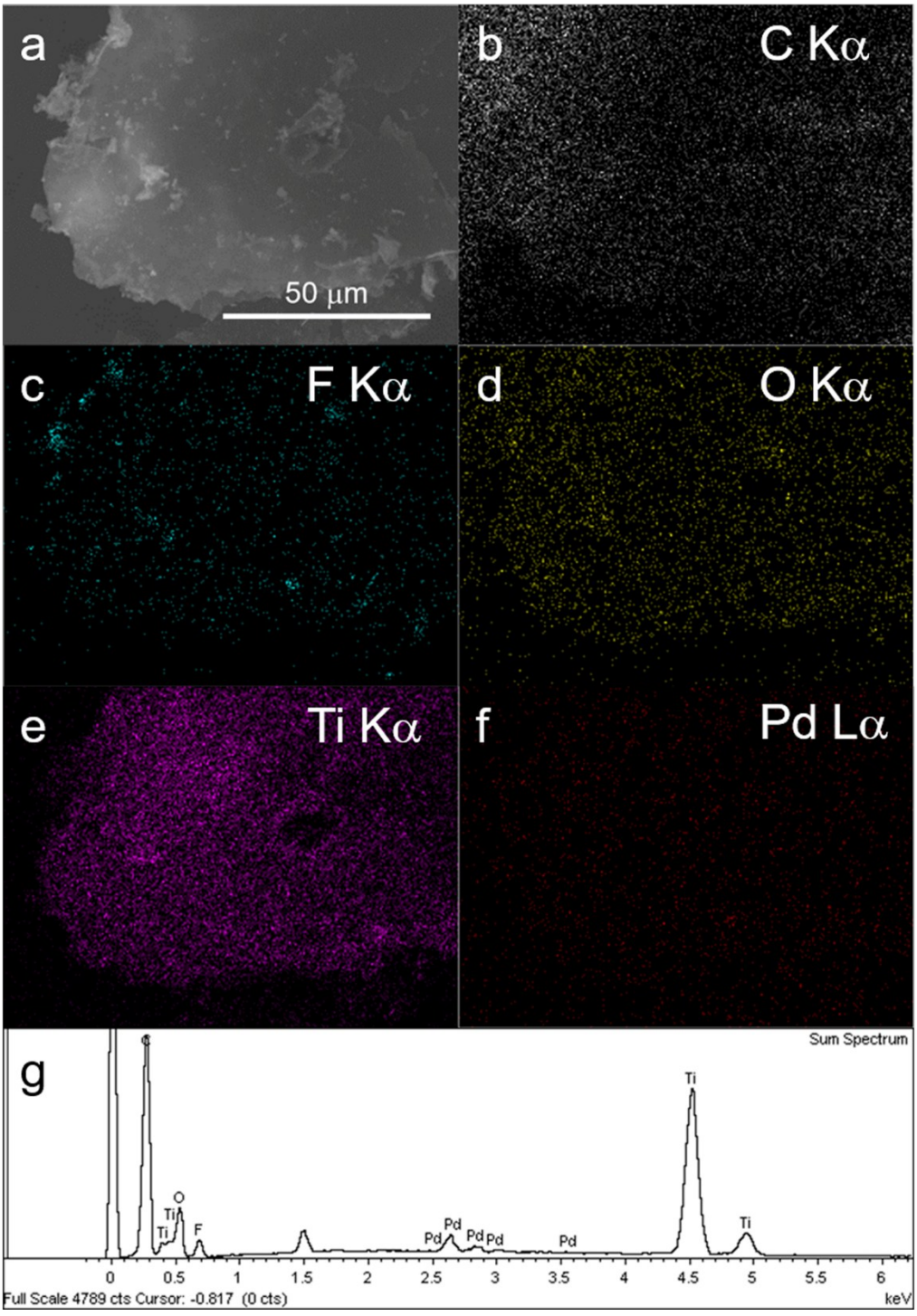

Fig. S4 a) SEM image, elemental distributions of b) C, c) F, d) O, e) Ti, f) Pd, and g) EDXS spectrum of Pd-MX.

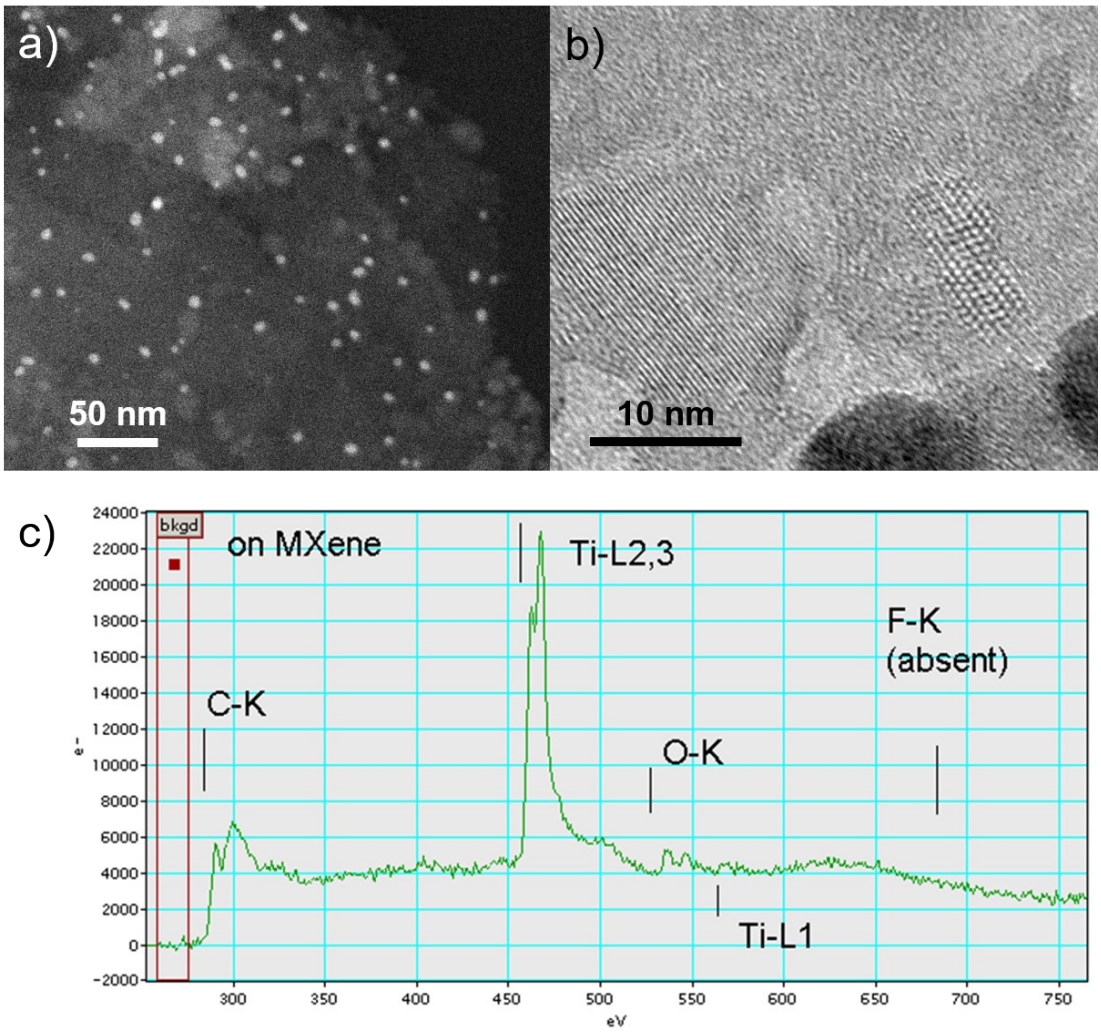

Fig. S5 a) STEM image, b) HRTEM image and c) EELS on MXene of Pd-MX.

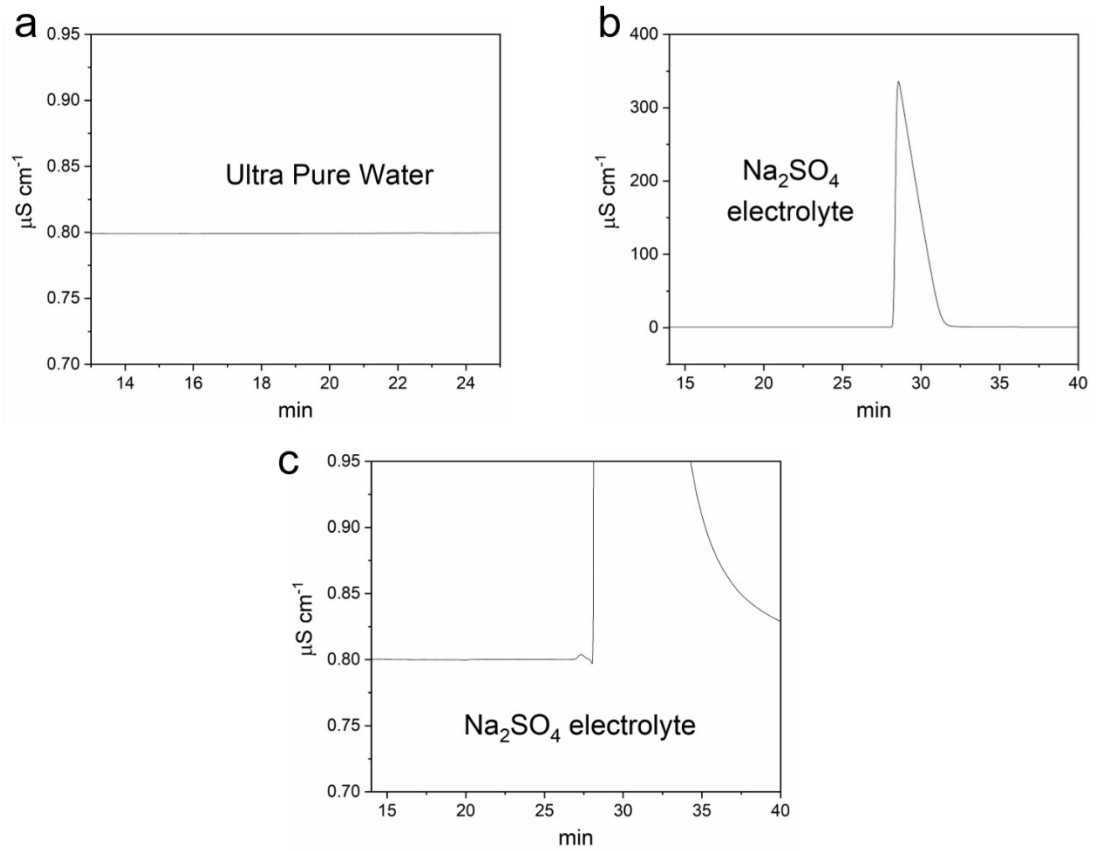

Fig. S6 Ion chromatogram spectra of a) ultra pure water, b) Na_2SO_4 electrolyte and c) Close-up view of b).

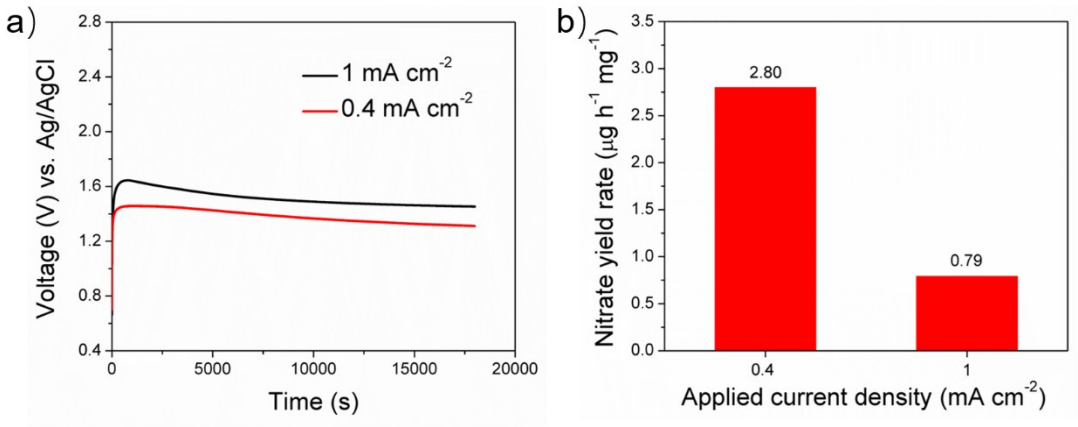

Fig. S7 a) Chronopotentiometry curves and b) nitrate yields of Pd-MXene electrode under NOR condition at the applied current density of 0.4 and 1 mA cm^{-2}, respectively.

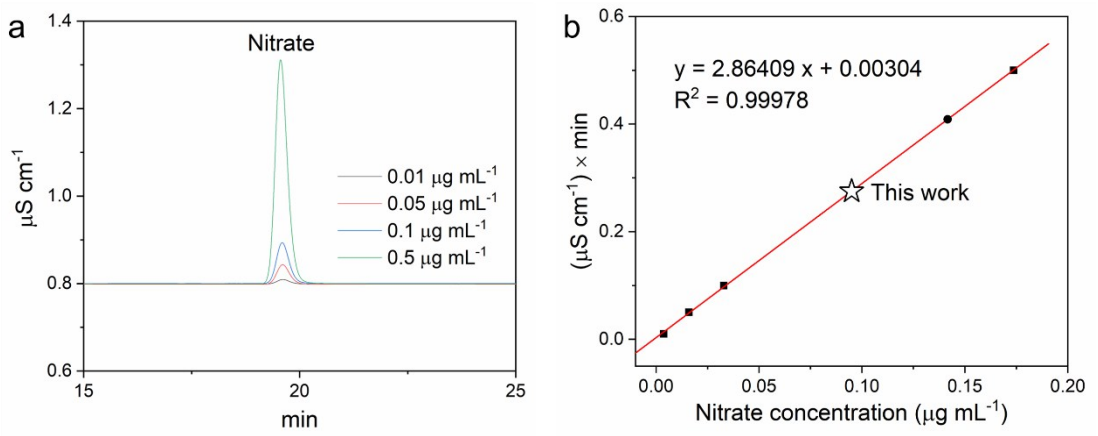

Fig. S8 a) Ion chromatogram (IC) spectra of standard nitrate solution. b) Calibration of standard nitrate ions by IC method. This work data comes from the test electrolyte (30 mL) by Pd-MXene for 5 h of NOR at 0.4 mA cm^{-2}.

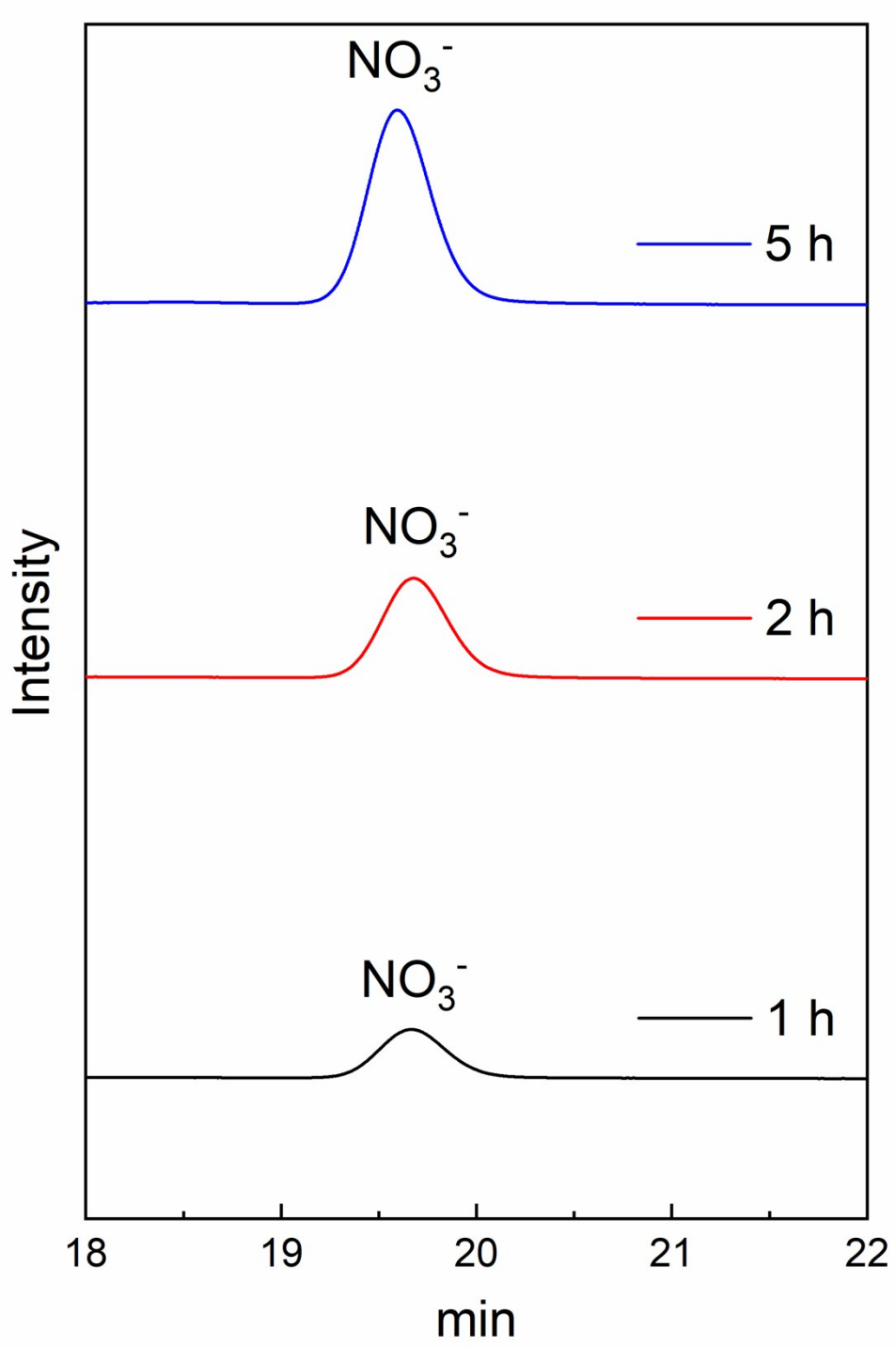

Fig. S9 The time-dependence of nitrate production in ion chromatogram spectra.

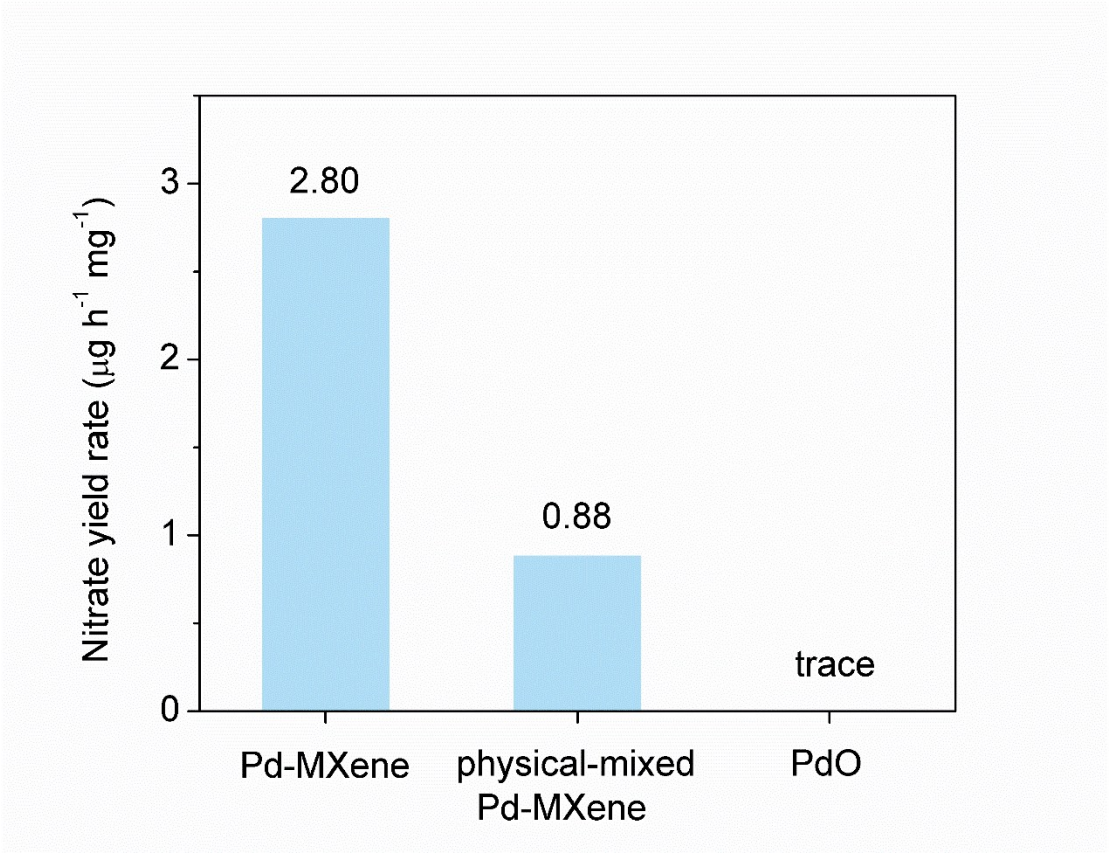

Fig. S10 Nitrate yield rates with assemble Pd-MXene, physical-mixed Pd-MXene and PdO at 0.4 mA cm^{-2} over 5 h of NOR.

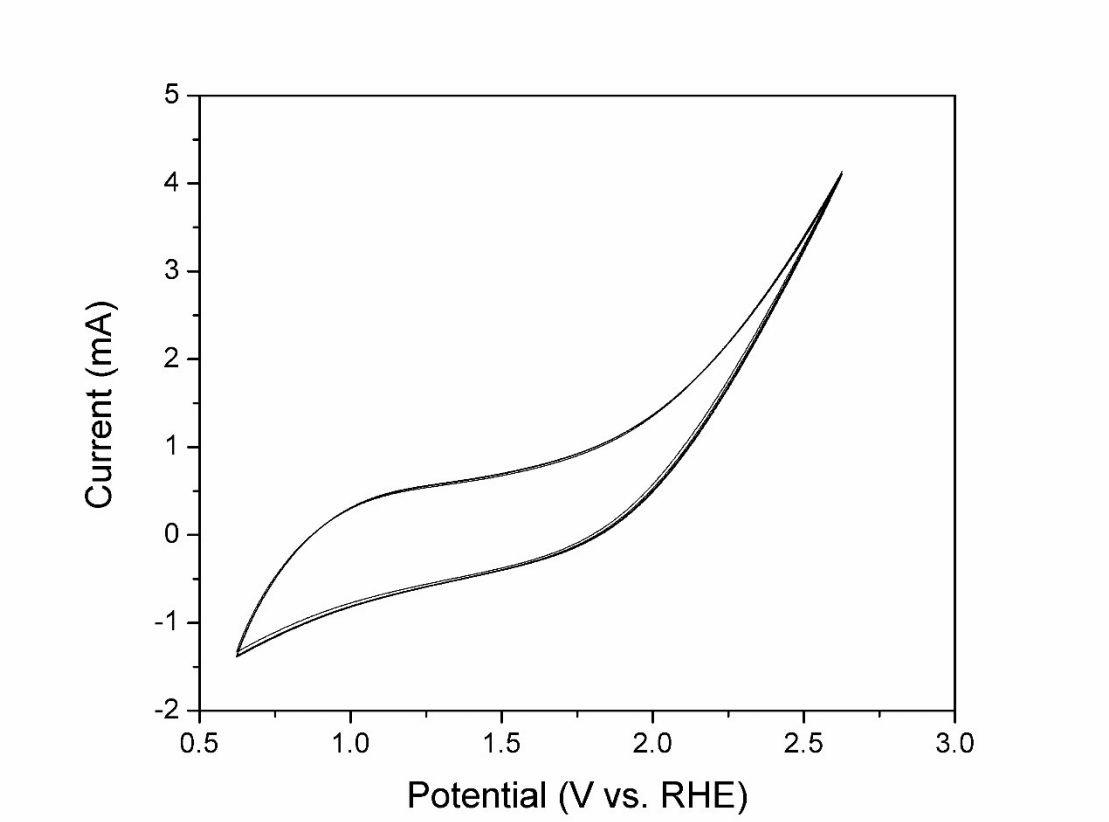

Fig. S11 Cyclic voltammetry curves of Pd-MXene at the potential range of 0.63-2.63 V vs. RHE.

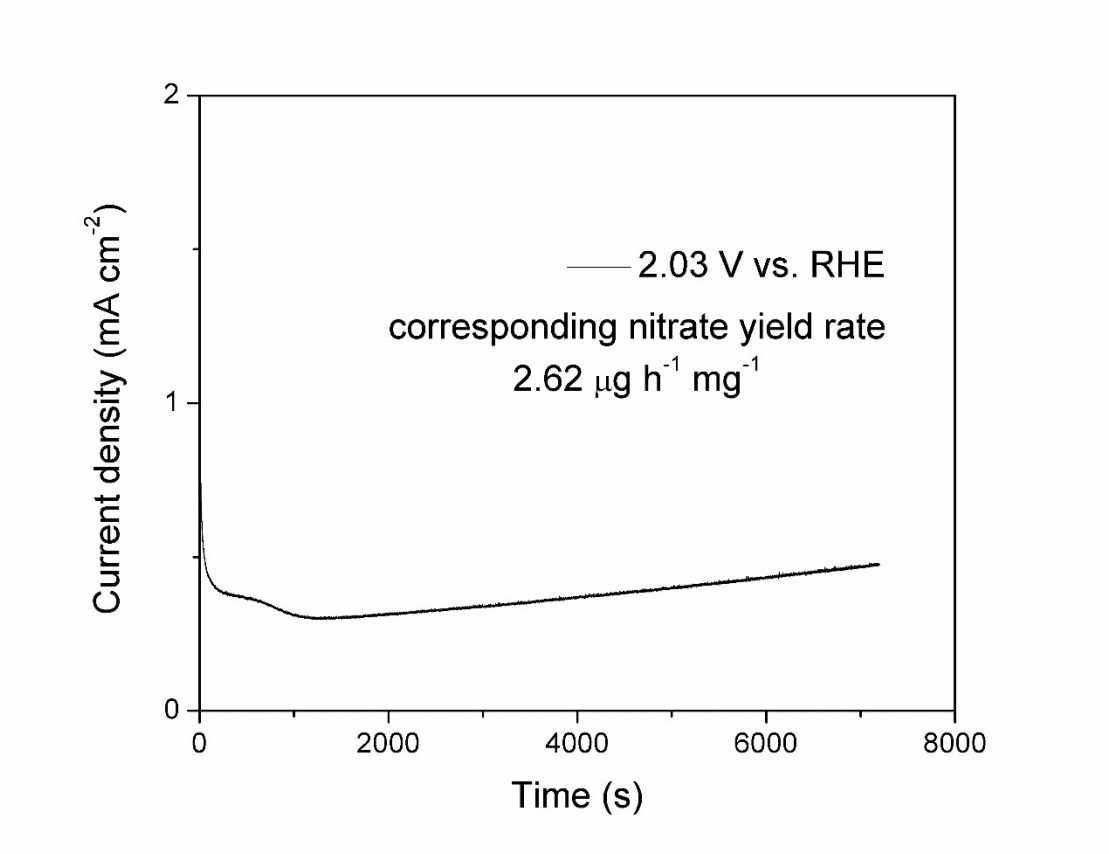

Fig. S12 Chronoamperometry curve of Pd-MXene at 2.03 V vs. RHE.

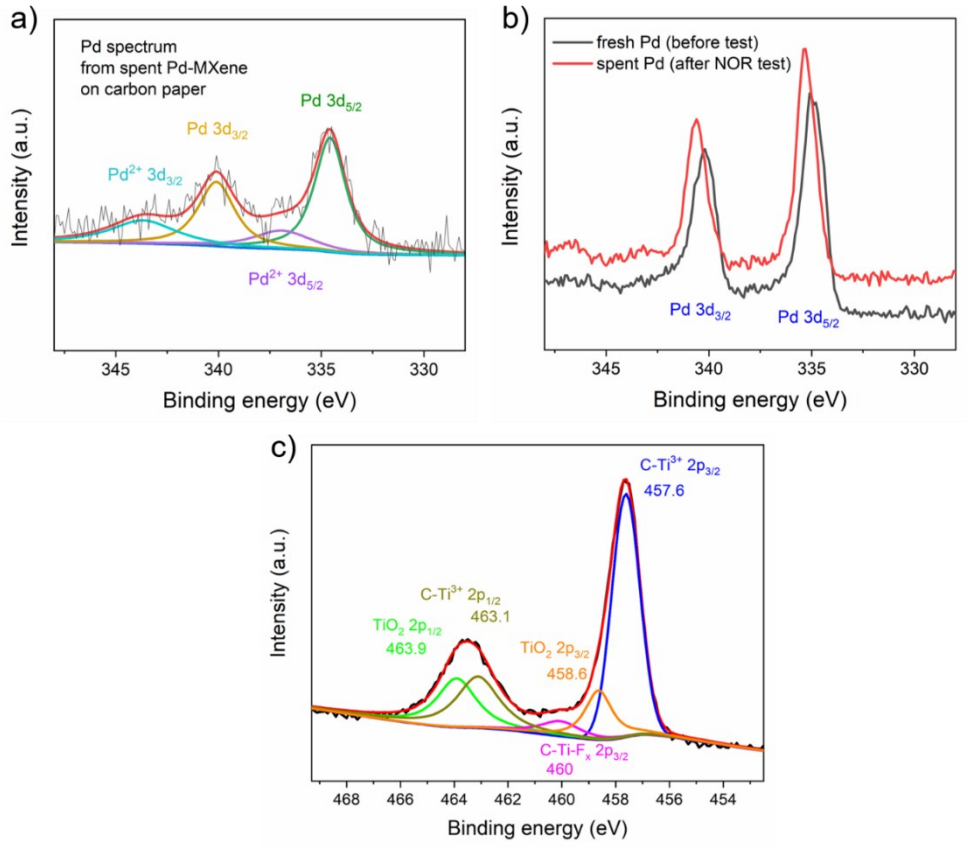

Fig. S13 XPS spectra of a) Pd 3d from spent Pd-MXene on carbon paper b) Pd 3d from spent Pd electrode and c) Ti 2p from spent Pd-MXene on carbon paper after 5 h of NOR at 0.4 mA cm^{-2}.

We choose Pd component as the NOR electrocatalyst mainly because Pd has been widely employed in a similar electrocatalytic ethanol oxidation system.[S3] Fig. 1h and Fig. S13a compare the oxidation state of Pd by XPS for fresh and spent Pd-MXene sample, and no obvious change was found under such small current density range (below 0.5 mA cm^{-2}). Furthermore, it is believed that the oxidation kinetics of Pd may be closely relate to the concentration of OH^- and corresponding current density, therefore the Pd oxidation process will be much slower in neutral condition with smaller current density than in alkaline condition with larger current density.[S4] Although MXene is easily oxidized in H_2O, it is thought that this oxidation will only occur at the surface, and further oxidation will be prohibited. Additionally, MXene-based electrocatalysts were well reported in OER process with good stability.[S5]
It is concluded that the slight oxidation of MXene was identified (Fig. S13c), while the oxidation of Pd was not obvious at the relatively low current density under NOR condition (Fig. S13a-b).

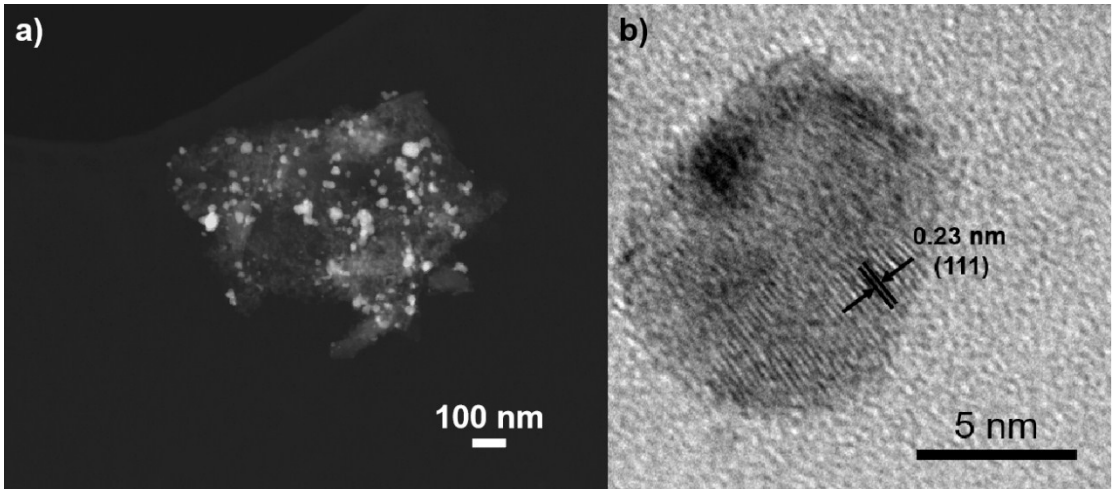

Fig. S14 a) Overview TEM image and b) HRTEM image of spent Pd-MXene after 5 h of NOR at 0.4 mA cm^{-2}.

HRTEM result indicates Pd particles (on MXene) remained most metallic (Pd^0) after NOR test at small current density.

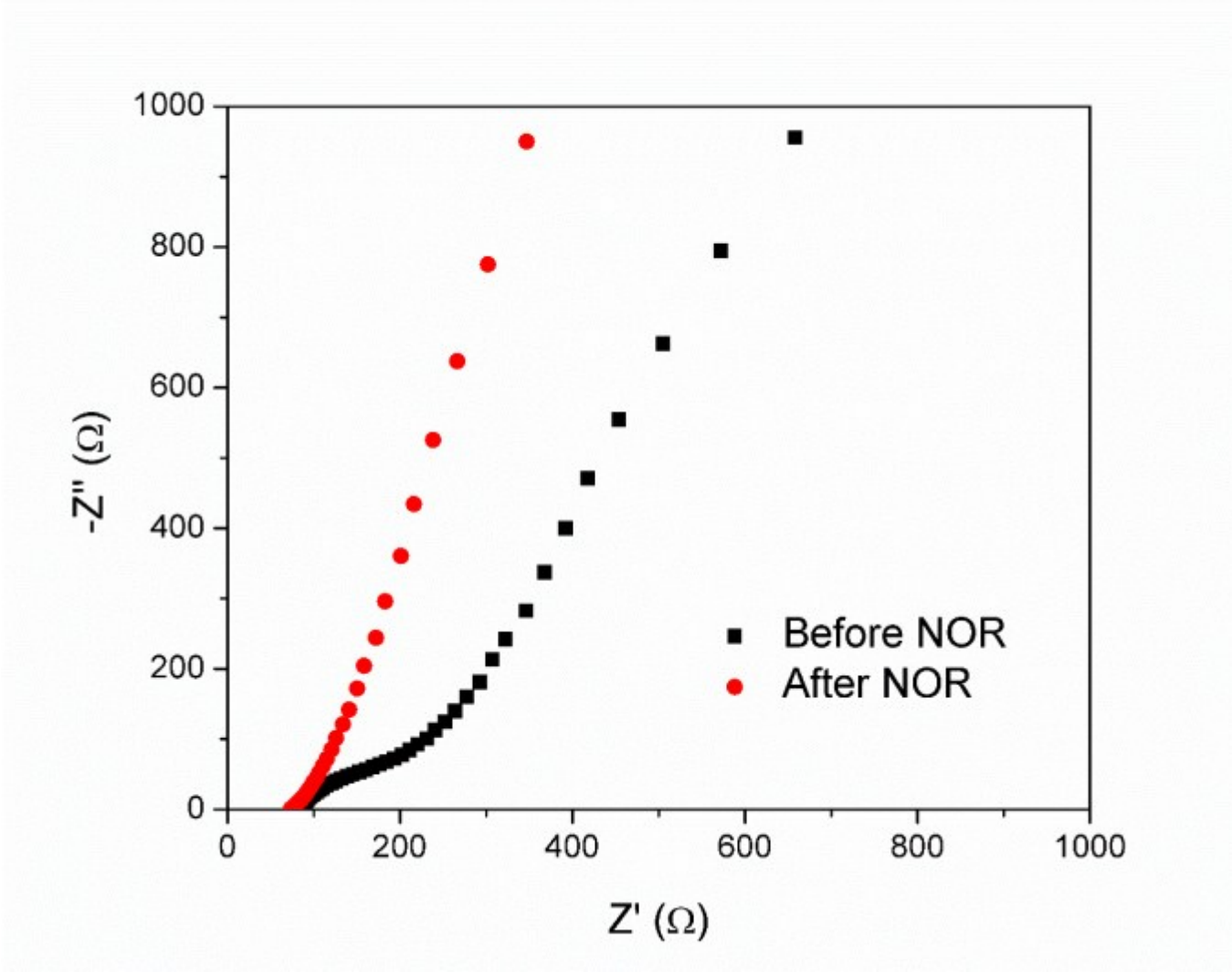

Fig. S15 EIS spectra from fresh and spent Pd-MX electrode (before and after 5 h of NOR test at 0.4 mA cm^{-2}).

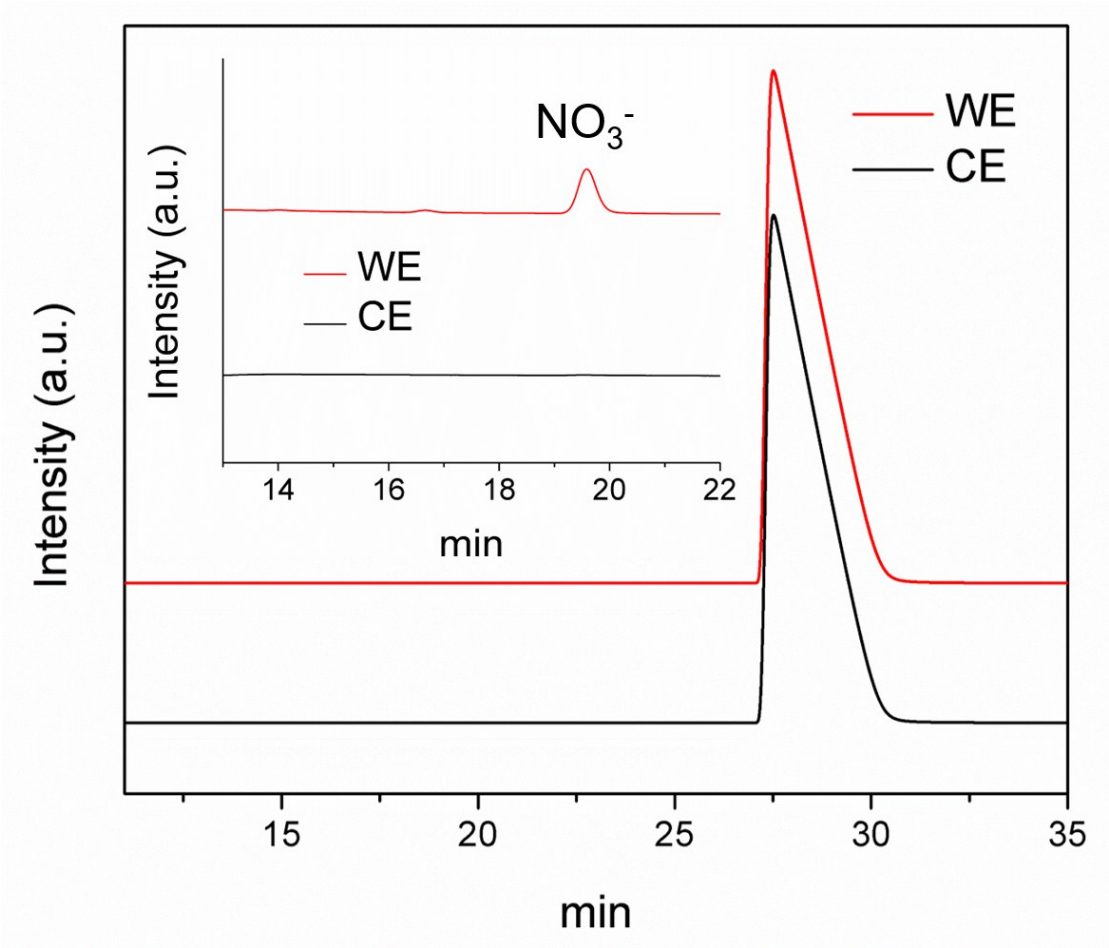

Fig. S16 Ion chromatogram spectra of the electrolytes from working-electrode side and counter-electrode side at 0.3 mA cm^{-2} for 5 h of NOR.

Sample	Ti concentration (ppm)	Pd concentration (ppm)
Fresh electrolyte	<0.1	<0.1
Used electrolyte	0.88	<0.1

Table S1 ICP analysis for fresh and used electrolyte after 5 h of NOR by Pd-MXene at 0.4 mA cm^{-2}.

ICP was used to analyse the compositional change of test electrolyte, and the increase of Ti element concentration was clearly observed, which demonstrates the catalyst loss (from carbon paper) may occur.

S3. NOR mechanism

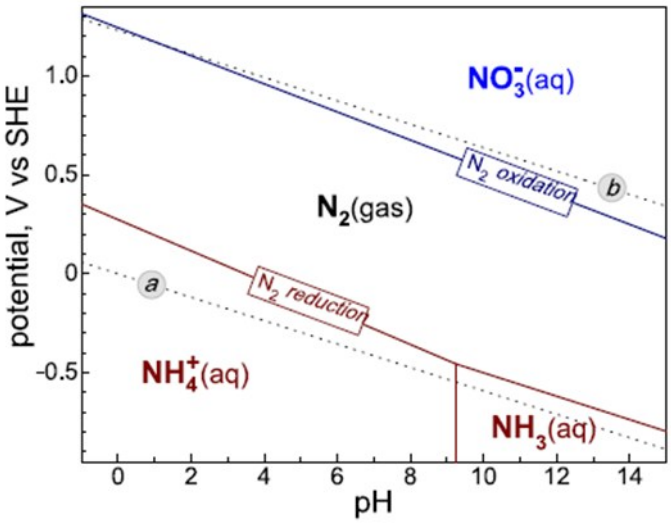

Fig. S17 Partial Pourbaix diagram for the N_2-H_2O system. Solid lines correspond to N_2 reduction to NH_4^+ or NH_3 and N_2 oxidation to NO_3^-. Dotted lines a and b straddle the region of water stability (reduction to H_2 and oxidation to O_2, respectively). Reprint from the reference.[S6]

Note that at pH > 1.3, NOR is more thermodynamically favorable than the parasitic OER. Thus, it is possible for NO_3^- to be the only product of an anodic process, particularly in neutral and alkaline solutions, if a sufficiently active and selective electrocatalyst can be discovered.[S6] Based on this assumption, we conduct our NOR experiment.

The conversion of N_2 to NO_3^- is proposed into two parts. The first part is the electrochemical conversion of N_2 to NO*, which includes the following reaction steps:

$$N_2 + * \rightarrow N_2* \qquad \text{Equation 3}$$

$$N_2* + OH^- \rightarrow N_2OH* + e^- \qquad \text{Equation 4}$$

$$N_2OH* + OH^- \rightarrow N_2O* + H_2O + e^- \qquad \text{Equation 5}$$

$$N_2O* + OH^- \rightarrow N_2O(OH)* + e^- \qquad \text{Equation 6}$$

$$N_2O(OH)* + OH^- \rightarrow 2NO* + H_2O + e^- \qquad \text{Equation 7}$$

where * denotes an active site on electrocatalysts. The second part is the conversion of NO* to NO_3^-, since the as-generated NO* can react with O_2

(produced by side OER reaction) and H_2O molecules to form NO_3^- via a non-electrochemical step at room temperature.

Recently, MacFarlane et. al. pointed out the selectivity problem existed in the electrochemical nitrogen reduction reaction (NRR), and concluded that limiting the hydrogen evolution reaction by supressing proton activity via using aprotic electrolyte like ionic liquid.[S7] However, no further universal approach has been reported till now for aqueous electrolyte based NRR (NRR selectivity<15%[S7]). With regards to NOR, OER and NOR will occur simultaneously at the very similar range of applied potentials/currents. Therefore, it is very difficult to tailor the aqueous electrocatalysis with promoted NOR but supressed OER. Lowering the overpotential will be deleterious to both NOR and OER kinetics, but may benefit to obtain a high nitrate Faradaic efficiency. The low selectivity of NOR is also closely related to low N_2 solubility in aqueous electrolyte. Overall, it is a big challenge to well balance the OER and NOR.

Reference

[S1] C. Du, K. N. Dinh, Q. Liang, Y. Zheng, Y. Luo, J. Zhang and Q. Yan, Adv. Energy Mater., 2018, 8, 1801127.
[S2] T. Ohno, F. Tanigawa, K. Fujihara, S. Izumi, M. Matsumura, J. Photochem. Photobiol. A: Chem. 1999, 127, 107.
[S3] C. Xu, H. Wang, P. Shen, S. Jiang, Adv. Mater. 2007, 19, 4256.
[S4] G. Wu, X. Zheng, P. Cui, H. Jiang, X. Wang, Y. Qu, W. Chen, Y. Lin, H. Li, X. Han, Y. Hu, P. Liu, Q. Zhang, J. Ge, Y. Yao, R. Sun, Y. Wu, L. Gu, X. Hong, Y. Li, Nat. Commun. 2019, 10, 4855.
[S5] T. Ma, J. Cao, M. Jaroniec, S. Qiao, Angew. Chem. Int. Ed. 2016, 55, 1138.
[S6] J. G. Chen, R. M. Crooks, L. C. Seefeldt, K. L. Bren, R. M. Bullock, M. Y. Darensbourg, P. L. Holland, B. Hoffman, M. J. Janik, A. K. Jones, M. G. Kanatzidis, P. King, K. M. Lancaster, S. V. Lymar, P. Pfromm, W. F. Schneider, R. R. Schrock, Science 2018, 873, eaar6611.
[S7] B. H. R. Suryanto, H. L. Du, D. Wang, J. Chen, A. N. Simonov, D. R. MacFarlane, Nat. Catal. 2019, 2, 290.